Laser and Particle Beams (2012), *30*, 583–590.
© Cambridge University Press, 2012 0263-0346/12 $20.00
doi:10.1017/S0263034612000663

On the interaction of focused electromagnetic beams and space-charge fields in laser-plasma systems

ALEXANDRE BONATTO, RENATO PAKTER, FELIPE BARBEDO RIZZATO, AND CRISTIAN BONATTO

Instituto de Física, Universidade Federal do Rio Grande do Sul, Porto Alegre, Rio Grande do Sul, Brasil

(Received 26 June 2012; Accepted 23 July 2012)

Abstract

In the present analysis we study the weakly nonlinear coupled dynamics involving focused radiation beams and space-charge fields in laser-plasmas systems. We direct the analysis to regimes evolving with the co-moving coordinate of the beam frame, but do not make any assumptions on paraxial or underdense conditions. The model thus constructed allows us to investigate equilibrium and nonequilibrium regimes alike. Dependence of equilibrium profiles on control parameters is examined, and beam stability and evolution is investigated as one adds small mismatches to the ideally matched equilibrium. Details of beam evolution depend on initial conditions. However, independently of the precise form of initial conditions, mismatched beams evolve to incoherent space-time patterns.

1. INTRODUCTION

The recent developments of laser technologies allow the creation of intense laser beams. As these beams are injected into plasmas, ponderomotive forces associated with the laser field eventually create charge displacement and the resulting space-charge fields. Space-charge fields and relativistic effects associated with the particle motion under the laser field contribute to beam focusing and pulse propagation, which allows the beams to be conveniently shaped for a large number of applications. Among these relevant applications one can think of nonlinear optics, communications, ionospheric propagation, laser fusion, particle and photon acceleration, and several others that make use of the nonlinear and geometric features of this type of systems (Kozlow *et al*., 1979; Tajima & Dawson, 1979; Shukla *et al*., 1986; Esarey *et al*., 1998; Farina & Bulanov, 2001; Mendonça, 2001; Poornakala *et al*., 2002; Bingham, 2003; Joshi & Katsouleas, 2003; Sodha *et al*., 2007).

When the beam modulational frequency and dimensions match the plasma wave frequency and wavelength, laser-plasma interactions are enhanced, which results in the generation of strong space-charge electric fields. These fields are relevant for the beam propagation itself and are of special interest for specific scenarios, as in particle acceleration where witnesses electrons traveling near the pulse velocity can be efficiently accelerated by wave-particle effects.

The previous remarks establish the importance attached to the study of the interaction of electromagnetic and space-charge waves in plasmas, and the variety of respective works reported in the literature is, accordingly, large. Indeed, interest areas range from time dependent regimes to regimes where field amplitudes depend only on the co-moving coordinates of a beam frame traveling with the group velocity of the radiation, all in various dimensionalities and various degrees of nonlinear approximations.

Analysis in the co-moving beam frame is of particular relevance for propagation over large distances, since after initial transients the radiation beams are attracted toward these co-moving regimes (Azimov *et al*., 1991). Here, analysis has been mostly done for planar propagation along one spatial dimension, where the finite dimensions of the transverse spot size are thus neglected. In this case, time and space are combined into a single co-moving beam frame coordinate where the dynamics is examined. Clear cut calculations can then be performed, as in the pioneering works of Kozlov *et al*. (1979) and de Bonatto *et al*. (2006), as well as in more recent works dealing with fully nonlinear relativistic cold fluid modeling (Farina & Bulanov, 2001; Poornakala *et al*., 2002; Bonatto *et al*., 2005). Although tools of nonlinear wave dynamics can be successfully applied in the analysis of one-dimensional geometries, the role of a possible transverse profile remains unclear.

Address correspondence and reprint requests to: Alexandre Bonatto, Instituto de fisica, Universidade Federal do Rio Grande do Sul, Caixa Postal 15051, Port Alegre 91501-970, Brasil. E-mail: abonatto@if.ufrgs.br

https://doi.org/10.1017/S0263034612000663 Published online by Cambridge University Press

That said, we can state that the purpose of the present work is to examine propagation of focused beams, where the dependence on transverse dimensions are kept alongside with the original dependence on the co-moving longitudinal coordinate. In other words, although our model restricts investigation to co-moving regimes, paraxial approximations are not imposed. A weakly nonlinear model is developed that allows us to represent the problem in terms of two nonlinearly coupled equations: one for the amplitude of the laser field, and another for the space-charge field. The goal is to describe the transverse beam profile as a function of the co-moving beam frame coordinate. As the model is constructed, no assumptions are made on the magnitude of the plasma density, as well. In particular, the model does not approximate the group velocity by the speed of light even at low-densities, as occasionally done in underdense conditions Duda & Mori (2000). Underdense and paraxial approximations suppresses some features we shall preserve along the analysis of beam equilibrium and dynamics (Mora & Antonsen, 1997; Esarey *et al*., 2000; Bonatto *et al*., 2011).

The paper is organized as follows. In Section 2, we present the model, discuss its geometrical settings and derive some analytical results, in Section 3, we numerically investigate the model examining its linear approximation, equilibrium solutions, and its nonlinear space-time dynamics, and in Section 4, we draw our conclusions.

2. THE MODEL

2.1. Governing Equation in the Weakly Nonlinear Approximation

Let us consider our system as consisting of a mobile cold electronic fluid and a neutralizing fixed ionic background.

In the co-moving regime we will be investigating, all field amplitudes, radiation, and wakes, are assumed to propagate along the x axis of our coordinate system with a given nonlinear group velocity v_g whose magnitude must be found.

Starting with the laser field, we take it to be described by the associated vector potential $\mathbf{A}$, which is represented in the form

$$\mathbf{A} = \hat{\mathbf{z}} a(\mathbf{x}_\perp, x - v_g\, t) e^{i(k_0 x - \omega_0 t)} + c.c. \tag{1}$$

The variable a is the slowly varying real amplitude of the field, with k_0 and ω_0, respectively, as the wave vector and frequency of the high-frequency carrier. We note that in accordance with all the previous comments on the field structure, in addition to the co-moving coordinate $\xi \equiv x - v_g\ t$, we allow for the inclusion of the transverse structure represented by the transverse coordinate $\mathbf{x}_\perp$ in the argument of the scalar amplitude a. The interdependence of the carrier's frequency and wave vector with the group velocity v_g, shall be elucidated as soon as one solves the wave equation for the vector potential $\mathbf{A}$.

In the Coulomb gauge, the laser wave equation reads

$$\frac{1}{c^2}\frac{\partial^2 \mathbf{A}}{\partial t^2} - \nabla^2 \mathbf{A} = \mu_0 \mathbf{j}, \tag{2}$$

where the high-frequency current $\mathbf{j}$ can be written in terms of the density n, the electron charge and mass q, m, respectively, the relativistic factor γ, and the vector potential as $\mathbf{j} = -(q^2/m)\, n\, \mathbf{A}/\gamma$ Gibbon (2007). Then, from Eq. (2) one can write the governing equation for the weakly relativistic amplitude a in the form

$$-(k_0^2 - \omega_0^2 + 1)a - 2i(\omega_0 v_g - k_0)\frac{\partial a}{\partial \xi} - (v_g^2 - 1)\frac{\partial^2 a}{\partial \xi^2} + \nabla_\perp^2 a = (n - \frac{a^2}{2})a. \tag{3}$$

We point out that in Eq. (3) we have migrated to dimensionless quantities defined in the form $\omega_p\, x/c \rightarrow x$, $\omega_p\, \mathbf{x}_\perp/c \rightarrow \mathbf{x}_\perp$, $\omega_p\, t \rightarrow t$, $qa/mc^2 \rightarrow a$, $v_g/c \rightarrow v_g$, and $(n - n_0)/n_0 \rightarrow n$. The parameter n_0 is the equilibrium density, $\omega_p = n_0\, q^2/\epsilon_0\, m$ denotes the plasma frequency, and μ_0 and ϵ_0 are the magnetic and electric vacuum permeabilities. We note that the frequency and wave vector of the carrier are normalized likewise, and that the weakly nonlinear (or weakly relativistic) field magnitudes satisfy the condition $|qa/mc^2| \ll 1$. On the right-hand side of Eq. (3) the nonlinear features of the theory can be devised: the ponderomotive nonlinearity represented by the coupling involving density and vector potential, and the cubic relativistic nonlinearity, which has its origins in the weakly relativistic expansion of the relativistic factor γ.

One can advance a step further with the analysis as one realizes that a is real. Then, on separating Eq. (3) into its real and imaginary parts the following expressions are obtained,

$$-\delta a + \kappa \frac{\partial^2 a}{\partial \xi^2} + \nabla_\perp^2 a = \left(n - \frac{a^2}{2}\right)a, \tag{4}$$

$$v_g = \frac{k_0}{\omega_0}. \tag{5}$$

The detuning parameter, introduced as $\delta \equiv k_0^2 - \omega_0^2 + 1$, is thus seen to be part of a nonlinear equation. As we shall elaborate better in the coming sections, this indicates that wave frequency and wave vector are related through a nonlinear dispersion relation, and that v_g is thus a nonlinear group velocity. On the other hand, the parameter $\kappa \equiv 1 - v_g^2$, here defined in a slightly different way than in a previous paper (Bonatto *et al*., 2011) to avoid negative values for it, is directly related to the group velocity of the radiation. It becomes small in underdense conditions where the plasma density is small and $v_g \rightarrow 1$. In what follows, we consider $\omega_0 > 0$, $k_0 > 0$, and $v_g > 0$.

https://doi.org/10.1017/S0263034612000663 Published online by Cambridge University Press

As for the low-frequency density fluctuations, one starts from the ponderomotive-driven low-frequency momentum equation for the electrons and uses the Poisson and continuity equations to obtain the following governing equation under the same set of normalizations previously employed:

$$v_g^2 \frac{\partial^2 n}{\partial \xi^2} + n = \frac{1}{2}\frac{\partial a^2}{\partial \xi^2} + \frac{1}{2}\nabla_\perp^2 a^2. \tag{6}$$

For convenience, we split the derivatives of the ponderomotive term on the right-hand side into longitudinal and perpendicular components.

We now proceed to reduce Eqs. (4) and (6) into a simpler and more amenable form for numerical and analytical investigations, avoiding underdense approximations where the velocity of the laser pulse is approximated by the speed of light.

Eq. (6) suggests a convenient combination of fields a^2 and n into a new quantity $\varphi \equiv v_g^2\, n - a^2/2$, which we call the space-charge potential. Accordingly, regrouping of terms in Eqs. (3) and (5) so as to replace $v_g^2\, n - a^2/2$ with φ, yields the following coupled equations for the laser field and for the space-charge potential, respectively:

$$\kappa \frac{\partial^2 a}{\partial \xi^2} = \delta a + \frac{1}{v_g^2}\varphi\, a + \frac{\kappa}{2v_g^2}a^3 - \nabla_\perp^2 a, \tag{7}$$

$$\frac{\partial^2 \varphi}{\partial \xi^2} + \frac{1}{v_g^2}\varphi = -\frac{1}{2v_g^2}a^2 + \frac{1}{2}\nabla_\perp^2 a^2. \tag{8}$$

The pair of Eqs. (7) and (8) casts itself into the convenient format we were looking for. If the transverse structure is neglected, the set becomes similar to models analyzed in the past (Mofiz & de Angelis, 1985). Under this planar condition, one can think of Eqs. (7) and (8) as describing the coupled nonlinear dynamics of fields a and φ as a function of the co-moving coordinate ξ, which plays the role of time. With the transverse structure included, the set of Eqs. (7) and (8) describes the weakly nonlinear full spatio-temporal interaction of laser and space-charge field. Coordinate ξ can still be seen as time, and space is associated with the transverse structure itself. We also point out that, in the present regime where fields depend on time through the co-moving coordinates, the presence of the nonparaxial derivative with respect to ξ in Eq. (7) is the chiefly responsible for advancing the laser field in time.

2.2. Beam geometry, Boundary Conditions and the Linearized Model

We first of all observe that solutions to the nonlinear Eqs. (7) and (8) depend on the geometry of the beam. In the present investigation, we adopt a slab geometry where the beam is uniform along one transverse cartesian axis, say z, and is localized along the other one, which we call $x_\perp$. This option avoids issues related to the inherent singularities at the axis of a cylindrical beam, but is nevertheless qualitatively similar to the cylindrical case if one looks at the half space $x_\perp \geq 0$, provided that the beam is symmetrical with respect to $x_\perp = 0$.

In summary, we require that all fields are even functions of the transverse coordinate $x_\perp$, vanishing as $|x_\perp| \to \infty$.

With the geometry and boundary conditions thus defined, we can make progress toward the solution as we note that the linearized version of set (7) and (8)

$$\kappa \frac{\partial^2 a}{\partial \xi^2} = -\nabla_\perp^2 a, \tag{9}$$

$$\frac{\partial^2 \varphi}{\partial \xi^2} + \frac{1}{v_g^2}\varphi = 0. \tag{10}$$

has an analytical solution. φ indeed oscillates with linear frequency $1/v_g$ while a can be resolved as

$$a(x_\perp, \xi) = a_0 e^{\left[\left(\frac{\lambda}{\kappa}\right)\xi^2 - \lambda x_\perp^2\right]} \cos\left(\frac{2\lambda\, x_\perp \xi}{\sqrt{\kappa}}\right), \tag{11}$$

if one Fourier analyzes Eq. (9) along its transverse coordinate $x_\perp$ and considers a general, initially static condition expressing the idea of localization or focusing: $a(x_\perp, \xi = 0) = a_0\, e^{-\lambda x_\perp^2}$, from where one can clearly see that the dimensional version of λ has the same dimension of $1/x_\perp^2$. Here we take $\delta = 0$ for simplicity, but this condition suffices for future purposes.

Eq. (9) is an elliptic equation similar to the Laplace equation, and its solution, Eq. (11), exhibits the expected exponentially growing behavior along ξ with the characteristic scale given by $\xi^* \equiv \sqrt{\kappa/\lambda}$. As nonlinear terms are added to the model, the exponential growth is likely to be saturated at some point. Our interest in what follows is to understand the competing roles of nonlinearity and the intrinsic exponential growth associated with the linear approximation. For further purposes, we point out that the exponential growth along the beam frame coordinate ξ can be seen as a spatio-temporal growth in the laboratory coordinates.

To conclude this section, we simply emphasize that the set (7) and (8) represents our basic model and provides the tools to analyze a myriad of problems, like soliton formation, wakefield excitation, and laser focusing.

Among these various problems, the present paper discusses initially focused beams and their subsequent dynamics.

3. NUMERICAL ANALYSIS OF FOCUSED BEAMS

3.1. Equilibrium Solutions

The equilibrium focused beam is the one where the beam transversal profile does not depend on the longitudinal "time" variable ξ. If this is the case, one can promptly

https://doi.org/10.1017/S0263034612000663 Published online by Cambridge University Press

write down from Eq. (8) the following expression for the space-charge potential ϕ in terms of the laser field:

$$\varphi = -\frac{1}{2}a^2 + \frac{1}{2}v_g^2\nabla_\perp^2 a^2. \tag{12}$$

Eq. (12) also represents the space-charge field under adiabatic conditions, where the the plasma wave frequency is much larger than the typical modulational frequency of the driving laser field.

The potential φ thus obtained from Eq. (12) can be inserted into Eq. (7) to generate the following differential equation for the equilibrium laser beam:

$$\nabla_\perp^2 a = \delta a - \frac{1}{2}a^3 + \frac{1}{2}a\nabla_\perp^2 a^2. \tag{13}$$

If from Eq. (13) we wish to create a radiation beam symmetrical with respect to the transverse coordinate, suffice is to work in the half-space $x_\perp \geq 0$, demanding that $da/dx_\perp|_{x_\perp=0} = 0$ and that $a(x_\perp \to \infty) \to 0$. Denoting a_{eq} as the equilibrium solution, the problem thus formulated admits an analytical solution of the form

$$a_{eq}^{analytical} = \sqrt{4\delta}\,\mathrm{sech}\left(\sqrt{\delta}x_\perp\right), \tag{14}$$

when the nonlinear term containing the Laplacian is ignored. We see from Eq. (14), for instance, how both amplitude and transverse length at equilibrium scale with the detuning δ. In particular, since δ defines the field amplitude, the frequency and wave vector of the carrier are related by a nonlinear dispersion relation, as alluded to earlier. The detuning δ (whose dimensional version has the same dimension of $1/x_\perp^2$), can also be seen as playing the role of the length scale λ at equilibrium.

The analytical solution is far from being inaccurate, because the discarded term leading to it is small. However, since we shall be dealing with unstable equations in the dynamics, it is recommended that all terms be kept. With all terms included, we take the following numerical procedure to construct solutions. Imposing the zero derivative condition at $x_\perp = 0$, we search for an initial amplitude $a_0 \equiv a(x_\perp = 0)$ that causes a to asymptotically approach zero as $x_\perp$ grows. The numerically found solutions will tend to and stay close to zero for a long stretch along the $x_\perp$-axis, but will eventually depart from this smallness condition. Numerical accuracy can be improved if we work out the digits of a_0 in such a way that the solutions asymptotically stay close to $a = 0$ for increasingly longer stretches.

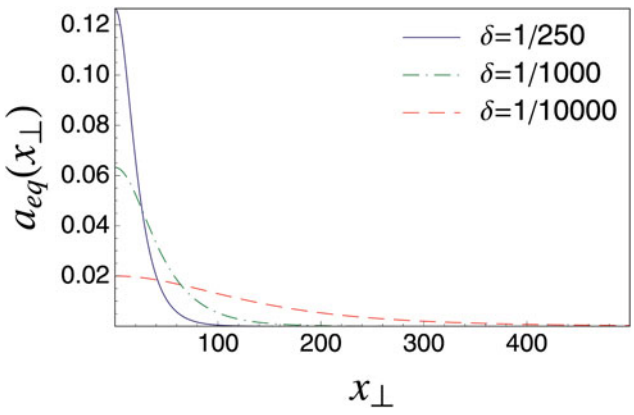


Fig. 1. (Color online) Plots of $a_{eq}(x_\perp)$ versus $x_\perp$ for various values of the detuning factor δ.

In Figure 1, we display a series of curves of a_{eq} $(x_\perp)$ versus $x_\perp$ for different values of the detuning parameter δ, the only control parameter present in the equilibrium equation (14). The detuning δ must be positive to generate a nontrivial solution, but small to guarantee smallness of field a_{eq}. We nevertheless see from Figure 1 that even for small detunings, the field profile largely varies with their exact values. As one moves from smaller to larger values of δ, the profiles become sharper, with larger amplitudes and narrower widths.

Once the equilibrium solutions have been found, we are in position to investigate the system behavior when initial conditions are launched in the neighborhood of these equilibria regimes. In other words, how does a mismatched radiation beam evolve as a function of beam-frame coordinate ξ? We address this issue as our next section.

3.2. Simulations of the Spatio-temporal Dynamics

3.2.1. Initial Remarks and the Linear Dynamics

Before entering in the study of the complete system, one should perhaps conduct a test comparing the analytical solution provided by Eq. (11) with simulations of the linear version of Eqs. (7) and (8). This first test helps to tune up simulation parameters, so that the corresponding results become as accurate as possible. We point out that this kind of test is important, given the fact that the elliptic nature of our system demands high numerical precision.

Simulations make use of a uniform mesh along $x_\perp$ to evaluate the corresponding Laplacian with finite differences. The fields at each node are advanced in ξ with an adaptive Runge-Kutta time integrator. We use $N = 256$ to $N = 1024$ nodes, along with a tolerance factor of 10^{-10}, and the differences are minimal. The simulation shown in Figure 2a was done with $N = 512$ and indeed displays nice agreement with the analytical results of corresponding panel (b). We also use $\lambda = 0.0001$ and a slightly underdense case $\kappa = 0.5$. Note that in the regime we are investigating, the forward moving wave front is located at $\xi = 0$ and we look at fields behind it with $\xi < 0$. This is why we represent the "time" in terms of its absolute value $|\xi|$. Note that although we work in a underdense regime, the typical underdense approximation $v_g \to c$ is totally avoided, as promised in our introductory remarks.

https://doi.org/10.1017/S0263034612000663 Published online by Cambridge University Press

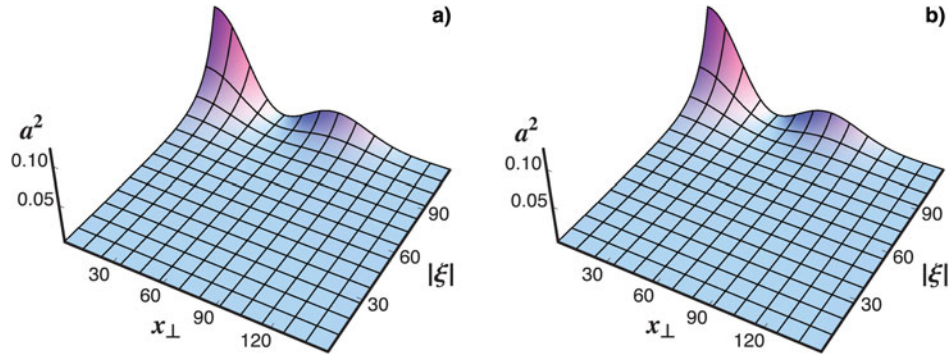


Fig. 2. (Color online) Comparing the space-time simulation code as applied to Eq. (10), panel (**a**), with the corresponding analytical result provided by Eq. (9), panel (**b**). We take $\lambda = 0.0001$ and $\kappa = 0.5$.

3.2.2. *Matched Beams*

Attention is next drawn toward the nonlinear spatio-temporal case. In our first look into the problem, we use the equilibrium solution yielded by the solution of Eq. (12) as the initial condition for our simulations based on Eqs. (7) and (8). The corresponding results are shown in Figure 3. One sees that the profile indeed remains unaltered for periods of time longer than the time scale ξ^* defined in the context of Eq. (11), which in our dimensionless form reads approximately $\xi^* \sim 70$ for the simulation parameters $\delta = 0.0001$, $v_g^2 = 0.5$ used here to illustrate the study. The growth scale is even shorter if one adds the destabilizing effects of the positive detuning absent in Eq. (11) but present in Eqs. (7) and (13)—the scale drops to $\xi^* \sim 50$. This fact suggests that the code, with all its nonlinear terms, remains robust against the known instabilities of the elliptic problem. As seen from our normalizations and from the approximate expression for equilibrium furnished by Eq. (13), the choice $\delta = 0.0001$ defines transverse length scales containing around 100 plasma wavelengths. This choice is quite compatible with experimental set-ups (Jha *et al.*, 2010) and shall be used throughout the paper.

3.2.3. *Mismatched Beams*

We finally address issues concerning the behavior of initially mismatched radiation beams. As we start off from nonequilibrium initial conditions, the interest is to see whether or not beams remain nearly focused if the initial mismatches are relatively small. In other words, a stability analysis shall be performed here.

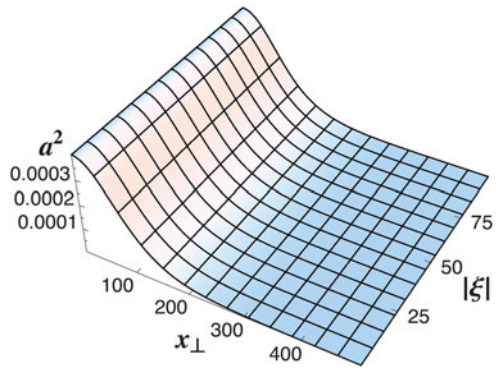


Fig. 3. (Color online) Testing the numerical code in equilibrium regimes. Here we take $\delta = 0.0001$ and $\kappa = 0.5$.

We had observed earlier that the linear version of our basic set is unstable in the sense that Eq. (9) predicts exponential growth for $a(x_\perp, \xi)$ as ξ advances. The reflex of this feature on the stability of equilibrium solution comes out as follows. If one takes the equilibrium solution a_{eq} for the laser field and perturb it with a small fluctuation $\widetilde{a}$ displaying sufficiently strong dependence on the transverse coordinate $x_\perp$, the equation governing $\widetilde{a}$ takes approximately the linear form already seen in Eq. (9):

$$\kappa \frac{\partial^2 \widetilde{a}}{\partial \xi^2} = -\nabla_\perp^2 \widetilde{a}. \tag{15}$$

Small perturbations thus grow with ξ, the signature of an unstable process. Even fields with more smoothly dependence on $x_\perp$ have spectral components at high values of the respective wave vector, so we expect instability in general, and not only when the dominant length scale of the perturbation is short.

The growing solution is eventually saturated by the nonlinear terms of the full set of equations, and we now attempt to offer a view of the whole process.

In Figure 4, we display several panels analyzing the time evolution of fields a and φ at various time scales along the ξ axis. The initially mismatched beam is written in the form

$$a(x_\perp, \xi = 0) = a_{eq}(x_\perp, \xi = 0) + \epsilon a_{eq}(\chi x_\perp, \xi = 0), \tag{16}$$

with $\varphi(x_\perp, \xi = 0) = \varphi_{eq}$. Fields a_{eq} and φ_{eq} are the equilibrium fields obtained in the previous subsection, $\epsilon \ll 1$ is a small parameter measuring the strength of the perturbing term, and χ is a scale factor indicating the dominant length scale of the perturbing term. Larger values $\chi > 1$ represent shorter transversal scales as compared to that of the equilibrium profile, and vice-versa. Let us consider $\delta = 0.0001$, $\chi = 10$, and $\epsilon = 0.2$ in all cases of Figure 4, with $\kappa = 0.5$

https://doi.org/10.1017/S0263034612000663 Published online by Cambridge University Press

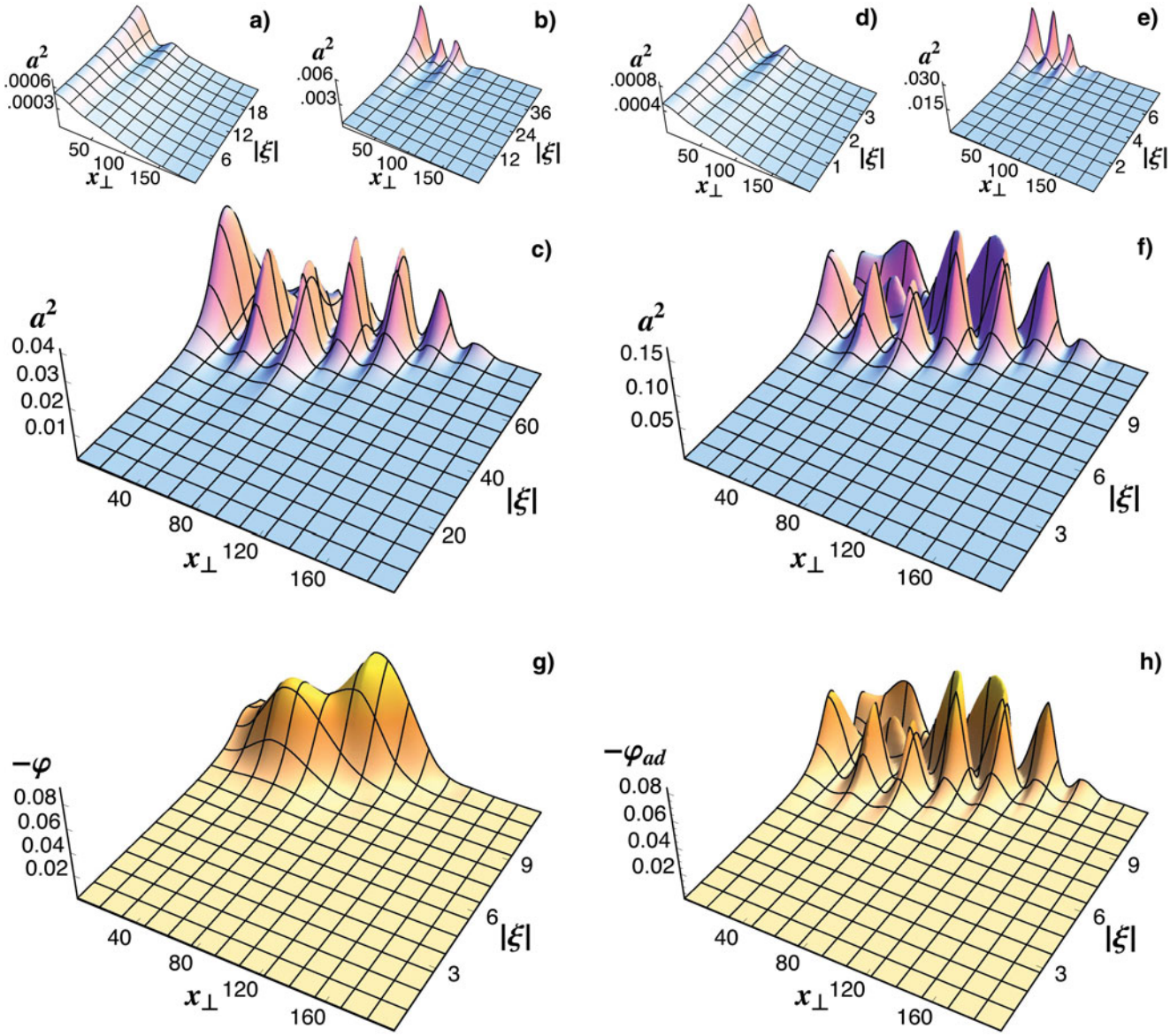


Fig. 4. (Color online) Full space-time history for the mismatched radiation beams at various time scales along the ξ axis, both in higher and lower density conditions. Panels (**a**) to (**c**) refers to laser amplitude in the higher density case $\kappa = 0.5$, and panels (**d**) to (**f**) to the laser amplitude in a low density underdense case $\kappa = 0.01$. In panels (**g**) and (**h**) the space-charge potential φ is shown for $\kappa = 0.01$; the actual potential in panel (g) follows the adiabatic dynamics of panel (h) only up to point where the beam breaks up. In all cases $\delta = 0.0001$ and $\chi = 10$.

for the first three panels, (a) to (c), and a more deeply underdense regime with $\kappa = 0.01$ for the last five panels (d) to (h). At the short times of panel (a) one can identify the exponential growing pattern typical of the linear regime for the laser field. Panel (b) still displays growing solutions and panel (c) finally reveals the saturation process following strong focusing near $x_\perp = 0$. As the initially growing mismatched solution reaches saturation, the beam breaks up into a seemingly irregular space-time pattern of beamlets and any coherence is lost. One sees that within the time scale displayed in Figure 4, the largest field amplitudes *a* lie quite within the weakly nonlinear regimes of laser wakefield accelerator settings (Mora & Antonsen, 1997). For longer times the irregular pattern progresses on, accompanied by spikes whose amplitudes lie beyond our weakly nonlinear assumptions.

Panels (d) to (f) represent a low-density case with $\kappa = 0.01$, which is more akin to underdense settings of wakefield accelerators, for instance. The laser patterns are similar to the previous case, but now one can notice that the development of the instability is much faster than the one seen in the $\kappa = 0.5$ case. Indeed, the scalings suggested in Eq. (6) indicate that, keeping the same initial profile (same λ), instability for the smaller value of κ should be approximately seven-fold faster than the one for the larger value.

In panels (g) and (h), we respectively compare the actual space-charge potential φ with its adiabatic approximation,

https://doi.org/10.1017/S0263034612000663 Published online by Cambridge University Press

let us call it φ_{ad}, earlier discussed in the context of Eq. (12). Given the initial smoothness of the radiation beam it is seen that the actual space-charge field initially follows an adiabatic dynamics, but only up to the point where the beam breaks up into the series of beamlets. Afterward the time scales for the wakes become comparable to the plasma wave scales. We use $\kappa = 0.01$ in panels (g) and (h).

As we mentioned, the above study for $\chi = 10$ represents those cases where initial mismatches have shorter length scales if compared to the length scale of the equilibrium profile. We commented that perturbations with longer length scales also grow, but still, it may be interesting to pinpoint the differences between the latter and former cases. The subject is examined in Figure 5, where we plot of curves of $a(x_\perp = 0, \xi)$ versus ξ for mismatched beams of the form given by Eq. (16). The cases $\chi = 10$ and $\chi = 0.5$ are compared for $\kappa = 0.01$, with all the remaining parameters as previously. Short length scales display the more conventional behavior of unstable cases: as the perturbation is created, the corresponding solution simply grows away from the equilibrium solution. However, when the long length scale represented by $\chi = 0.5$ is considered, the mismatched solution is initially attracted by the equilibrium and only then moves away as seen in the inset. The remarkable fact is that mismatches with long length scales behave like stable perturbations until one reaches the time scale of exponential growth, where the initial solution depart from the vicinity of equilibrium.

4. CONCLUSIONS

The present paper was devoted to the study of focused laser beams in laser-plasma nonlinear interactions.

We first developed the model and obtained the associated equations governing beam evolution in the co-moving beam frame. Nonparaxial terms were fully preserved, and care was taken to avoid underdense approximations where the group velocity of the radiation field is approximated by the speed of light in vacuum. With the resulting formalism, we investigated equilibrium conditions and space-time dynamics alike, all for arbitrary plasma densities.

We first observed that equilibrium beams display profiles that depend on the detuning factor δ. Similarly to the case of one-dimensional electromagnetic solitons, larger detunings correspond to higher amplitudes and narrower widths. We also observed that mismatched (or nonequilibrium) beams develop instabilities that are saturated by the nonlinear effects of the theory. The growth of the instabilities depend on details of the initial perturbation: long wavelength perturbations tend to display slower growths than short wavelength perturbations.

In general, we commented earlier that the factor $\kappa = 1 - v_g^2$ combines with the transverse length scale $1/\lambda$ to the form the "time" scale $\sqrt{\kappa/\lambda}$ for perturbations growing along the ξ axis. This means that lower density systems tend to evolve in time in a faster fashion than higher density ones as seen in the simulations. Even beams with smooth transversal profiles are subject to a relatively fast dynamics in sufficiently underdense conditions. If one takes, for instance, a beam with reasonable transverse size $\sim 50\ \mu m$ and plasma wavelength $\sim 0.5\ \mu m$, one falls close to the numerical parameters discussed in the paper. In this case, if $\kappa \sim 0.01$, one should see appreciable mismatched beam evolution within a few plasma wavelengths.

The initial conditions examined in the present work correspond to focused laser beams. However, as mentioned earlier, the present formalism can also tackle other types of initial conditions. One can, for instance, excite localized radiation bumps along the longitudinal axis and examine wakefield generation as these bumps move into the plasma. The relevance of this problem is well documented and a full investigation shall be reported in the near future.

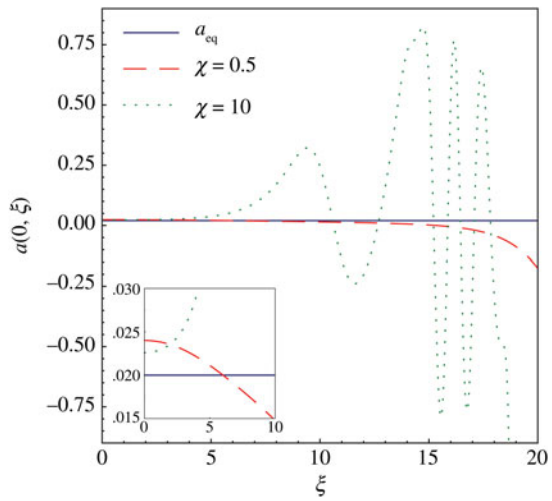


Fig. 5. (Color online) Dependence of the dynamical behavior on the mismatch scale χ. Longer scales tend to be display slower growths.

ACKNOWLEDGMENTS

We acknowledge support by CNPq, Brasil, and by AFOSR, USA, grant FA9550-09-1-0283.

REFERENCES

Azimov, B.S., Sagatov, M.M. & Sukhorukov, A.P. (1991). Formation and propagation of steady-state laser pulses in media under the combined action of third- and fifth-order nonlinearities. *Sov. J. Quant. Electron.* **21**, 93.

Bingham, R. (2003). Accelerator physics—In the wake of success. *Nat.* **424**, 258.

Bonatto, A., Pakter, R. & Rizzato, F.B. (2006). Nonlinear dynamics of electromagnetic pulses in cold relativistic plasmas. *J. Plasma Phys.* **72**, 179.

Bonatto, A., Pakter, R. & Rizzato, F.B. (2011). Self-consistent dynamics of electromagnetic pulses and wakefields in laser-plasma interactions. *Laser Part. Beams* **29**, 399.

https://doi.org/10.1017/S0263034612000663 Published online by Cambridge University Press

Duda, B.J. & Mori, W.B. (2000). Variational principle approach to short-pulse laser-plasma interactions in three dimensions. *Phys. Rev. E* **61**, 1925.

Esarey, E., Hafizi, B., Hubbard, R. & Ting, A. (1998). Trapping and acceleration in self-modulated laser wakefields. *Phys. Rev. Lett.* **80**, 5552.

Esarey, E., Schroeder, C.B., Shadwick, B.A., Wurtele, J.S. & Leemans, W.P. (2000). Nonlinear theory of nonparaxial laser pulse propagation in plasma channels. *Phys. Rev. Lett.* **84**, 3081.

Farina, F. & Bulanov, S.V. (2001). Relativistic electromagnetic solitons in the electron-ion plasma. *Phys. Rev. Lett.* **86**, 5289.

Gibbon, P. (2007). *Short Laser Pulses Interactions with Matter*. London: Imperial College Press.

Jha, P., Malvyia, A. & Upadhyay, A.K. (2010). Wakefield effects on the evolution of symmetric laser pulses in a plasma channel. *Laser Part. Beams* **28**, 245.

Joshi, C. & Katsouleas, T. (2003). Plasma accelerators at the energy frontier and on tabletops. *Phys. Today* **56**, 47.

Kozlov, V.A., Litvak, A.G. & Suvorov, E.V. (1979). Envelope solitons of relativistically strong electromagnetic waves. *Zh. Eksp. Teor. Fiz* **76**, 148.

Mendonça, J.T. (2001). *Theory of Photon Accelerator*. *Bristol*: IOP Publishing.

Mofiz, U.A. & de Angelis, U. (1985). Nonlinear propagation and localization of intense electromagnetic waves in relativistic plasmas. *J. Plasma Phys.* **33**, 107.

Mora, P. & Antonsen, T.M. Jr. (1997). Kinetic modeling of intense, short laser pulses propagating in tenuous plasmas. *Phys. Plasmas* **4**, 217.

Poornakala, S., Das, A., Sen, A. & Kaw, P.K. (2002)., Laser envelope solitons in cold overdense plasmas. *Phys. Plasmas* **9**, 1820.

Sodha, M.S., Sharma, A. & Agarwal, S.K. (2007). Focusing of electromagnetic beams in ionosphere with finite thermal conduction. *J. Geophys. Res.* **112**, A03302.

Shukla, P.K., Rao, N.N., Yu, M.Y., & Tsintsadze, N.L. (1986). Relativistic nonlinear effects in plasmas. *Phys. Lett.* **138**, 1.

Tajima, T. & Dawson, J.M. (1979). Laser electron-accelerator. *Phys. Rev. Lett.* **43**, 267.

https://doi.org/10.1017/S0263034612000663 Published online by Cambridge University Press